encit 2020

ABCM Associação Brasileira de Engenharia e Ciências Mecânicas

18th Brazilian Congress of Thermal Sciences and Engineering
November 16-20, 2020, (online)

ENC-2020-0045
THREE-DIMENSIONAL NUMERICAL INVESTIGATION OF A SCRAMJET INLET CONSIDERING MACH NUMBER VARIATION

João Vitor Marques Brito de Siqueira
Guilherme Borges Ribeiro
Instituto Tecnológico de Aeronáutica - Praça Marechal Eduardo Gomes, 50 - Vila das Acacias, São José dos Campos - SP, 12228-900
Joaovitormarques22@hotmail.com, guiborgesribeiro@gmail.com

Mauricio Antoniazzi Pinheiro Rosa
Instituto de Estudos Avançados - Trevo Coronel Aviador José Alberto Albano do Amarante 01 - Putim, SP, 12228-001
mauricioaprosa@gmail.com

Abstract. *This work has the purpose of investigating, through detailed three-dimensional computational fluid dynamics (CFD) analyses, the influence of Mach numbers on the airflow in a scramjet intake. This work focus on the influence Mach number has on the airflow and performance of the scramjet intake (compression ramps and isolator). Three cases with different Mach numbers have been considered in this work: Mach numbers of 6.8, 7.2 and 7.6. All the other parameters and boundary conditions are the same for these three cases. Mach number contour images and values of properties on the walls have been analyzed to obtain the conclusions present in this paper. Besides it, viscous effects due to the sidewall, and the influence these effects have on the airflow, are also investigated.. Higher Mach numbers also increase the total and static pressure.*

Keywords: *Scramjet, CFD, Mach number*

1 - INTRODUCTION

During the 21st century, a great number of loads are assumed to be taken into orbit. The cost to put something into orbit is enormous and therefore the development of an air-breathing engine as an alternative for hypersonic propulsion is required. The great advantage air-breathing engines have is that they don`t need the vehicle itself to transport the oxygen for the combustion, as it happens to rocket engines. The use of air-breathing engines enables the vehicle to decrease its volume and weight resulting in higher specific impulses (Heiser, 1994; Segal, 2009; Griffiths, 2005; Smart, 2008; Alcaide, 2007). The supersonic combustion ramjet (scramjet) has been conceived to operate in high altitude flights. Its theoretical top speed is between Mach numbers 12 and 24 (Segal, 2009). The ramjet engine features combustion in subsonic flow while the scramjet engine has its fuel combustion happening with air at supersonic speed. That difference brings up some technological challenges to develop a scramjet engine. When the airflow is decelerated by the scramjet engine, the relative velocity and kinetic energy decrease, and conservation of energy requires that any missing kinetic energy will reappear as internal energy, with the result that pressure, temperature, and density of the flow entering the burner are considerably higher than in the freestream. When the flight Mach number exceeds about 6, this effect becomes so pronounced that it is no longer advantageous to decelerate the flow to subsonic speeds (Heiser, 1994). As in any conventional thermal power cycle, in both engines, the flow is compressed. The airflow compression is done by oblique shock waves at the inlet and diffuser. After such compression in ramjet engines, the airflow becomes subsonic after passing by a normal shock wave and inside the burner happens subsonic combustion. On the other hand, in scramjet engines, the airflow goes to the burner in supersonic speeds. If velocities are increased too much, the normal shock wave that occurs inside the ramjet engine leads to hugely high pressure loss. Yet the temperature increases a lot causing structural stresses and chemical dissociation of the airflow, which makes the cycle to lose energy (Smart, 2008). The solution for it is to remove the normal shock and allow the airflow to enter the combustor in supersonic speeds, from where

comes the idea of the supersonic combustion ramjet, or scramjet. The fuel, in a scramjet engine, remains inside the burner for a really short time and therefore it is injected just downstream the diffuser to achieve a rapid and thorough mixing. Thus, the high pressure, hot flow is directed to the nozzle that, in the case of a scramjet engine, must be divergent once the airflow is supersonic. The after-combustion flow is then exhausted into de atmosphere and can also be accelerated by the vehicle after-body that can be used as an expansion surface. Scramjets are supposed to operate in hypersonic speeds, i.e. above Mach 5, and theoretical operational limits as high as Mach 24 (Segal, 2009).

The scramjet, as well as other air-breathing propulsion systems, needs to operate at ideal altitudes to produce great dynamic pressure necessary for maximum performance. Relatively low altitudes, for long periods, are not the ideal for proper operation of the scramjet engine once high dynamic pressure and high Reynolds numbers can cause uncertainty in the boundary-layer transition, large aerodynamic loads, and a great surface heating. These are the phenomena that, in general, determine the design of the vehicle (Bertin, 1994). The scramjet engine needs to operate at hypersonic airflow so that the engine inlet can produce oblique shock waves that compress the airflow to enable combustion and ideal operation of the engine. Hence, the scramjet engine can't take off by itself. A turbojet engine can accelerate the hypersonic vehicle at speeds that make possible the scramjet to reach hypersonic speeds. For missions beyond the earth's atmosphere, rocket engines need to be activated (Segal, 2009).

The subsequent step in this work, is the 3D numerical analysis of the whole inlet of a scramjet engine. Its inlet is composed by a forebody with three compression ramps (triple wedge) and an isolator, which has the purpose of only protecting the inlet from adverse back pressure in the combustor. This scramjet engine analyses considered 0.5 mm of forebody and cowl leading edge radii, isolator heights of 20 mm. Regarding the numerical details and boundary conditions, this work considered transitional viscous SST model, different wall conditions for the walls, 30 km of flight altitude and different Mach numbers. The advantage of three compression ramps is getting closer to an isentropic compression that maximizes the total pressure recovery inside the isolator (Heiser, 1994)

The desire for hypersonic flight in the atmosphere has driven many scientists and engineers throughout the years. In the late 1950s and 1960s, rocket engines were vastly used to access space, however, it was a common sense that only an airbreathing propulsion system would be able to provide a practical hypersonic flight cruise. The most suitable engine for this kind of flight is certainly the scramjet or supersonic combustion ramjet. The scramjet engine uses the shock waves generated at its intake to compress the airflow and enter the combustion chamber in supersonic velocities. The intake of scramjet engines plays an important role to enable efficient combustion and, therefore, has been extensively studied by many researchers in the last years. An example of a state-of-art work in this field is the one from Javed and Chakraborty (Javed, 2017), where they evaluated the side spillage for a hypersonic air intake using computational fluid dynamic techniques. The mass capture ratio of hypersonic air intake is one of the most important performance parameters. Javed and Chakraborty studied the intake of a non-axisymmetric scramjet engine, designed using stream thrust methodology, employing computational fluid dynamic techniques (CFD). A large amount of airflow is observed to spill from the sides and this is not considered in the initial design phase. There is no estimate of how much airflow is related to this spillage and computational fluid dynamic studies become the only possible tool to estimate the mass capture ratio. This shows that a critical loss in mass capture ratio without side walls is observed (68.17%) due to side spillage only. A sidewall is provided to hold the spillage and improves in 88,67% the mass capture ratio. Deterioration of flow parameters such as static temperature, Mach number, and the total pressure is observed in this analysis. Another example of scramjet intake researches is the work done by Seong-kyun Im and Hyungrok Do (Im S., 2018) , where they investigate the unstart phenomena induced by flow choking in scramjet inlet. For the same reasons discussed before, avoiding unstart conditions is one of the primary objectives when designing the scramjet inlet. This work investigates research progress in identifying flow choking mechanisms that can trigger unstart. Three different flow choking mechanisms are discussed: flow blockage, mass addition, and heat release from combustion reactions. The paper then presents some state-of-the-art methods to detect, prevent, and control unstart when present. This work then suggests that more investigations is needed in high enthalpy facilities that would certainly help to better understand the heat release-driven unstart. Another work that focused on the improvement of scramjet engines is the one from Sarout (Sarout et al, 2020) that worked on the numerical simulation of flow through scramjet intake. This paper focuses on the performance enhancement of the supersonic air intake model through the implementation of a pressure feedback system with different connecting locations. A Mach 5, supersonic air intake model with a larger shoulder separation and other two separations at cowl lip and inside the isolator is studied. This model has been simulated using CFD package Ansys Fluent-18. Three different pressure feedback configurations were examined to investigate the performance improvement of the intake system. Improvement in total pressure at the exit of the isolator is accomplished through the use of a pressure feedback system by greatly decreasing the boundary layer separation. This study found that the

flow through the pressure feedback system happens due to the pressure difference between the boundary layer separation and the upstream side regular flow. This pressure feedback system can reduce the intensity of shock wave boundary layer interaction and the size of the separation occurring at the isolator entry section, cowl lip, and inside the upper part of the isolator. This study demonstrates the scope of overall improvement in scramjet engine performance through the use of a pressure feedback system. Senthilkumar (Senthilkumar et al., 2017) studied the effect of cowl angle in the performance of scramjet air intakes. Shock-Wave Boundary Layer Interaction (SWBLI) is an unwanted phenomenon that happens inside the scramjet intake which has a detrimental influence on its performance.

Because of the adverse pressure gradient generated by SWBLI, the flow can be decelerated to subsonic speeds via normal shock. This leads to engine unstart of the engine including other undesirable phenomena such as high drag and increased localized heating. This work focuses on study, through computational fluid dynamics, how the change in cowl angle can help to prevent such phenomena. It was found that the increase of the angle of attack of the cowl decreases the size of boundary layer separation at the cost of a loss in total pressure and intake unsteadiness. Another worth mentioning work is the one from Siqueira (Siqueira et al., 2020). In this work, it was numerically examined the evaluation of effects of the isolator height and leading-edge bluntness on a scramjet intake. Hypersonic speeds make the temperature and heat flux to increase a lot on leading edges. In this way, the scramjet intake must feature blunt leading edges. This work considers three leading-edge radii: sharp, 0.5, and 1.0 mm. Besides it, isolator height was also investigated. Two heights were considered: 15 and 20 mm. It was evidenced that both leading-edge bluntness and isolator height greatly influence the intake airflow structure. Results showed that the isolator height had a major effect on the flow separation at the isolator entrance yielding a recirculation zone that increases with the isolator height. Furthermore, higher Stanton numbers and temperature along the isolator were found for the shorter isolator height due to stronger shock waves and higher frequency of shock-wave train. Regarding the analysis of the leading-edge bluntness, Siqueira et al found out that the heat flux decreases on the leading edges as the radius increases. Nevertheless, a decrease in the adiabatic kinetic efficiency was observed when the leading-edge radius was increased. Moreover, blunt leading edges promoted a decrease in heat flux along the scramjet intake walls and also a decrease in average temperatures throughout the isolator. One last example is of state-of-art research in developing scramjet intakes is the work proposed by Zhu (Zhu et al, 2018) that designed a three-dimensional hypersonic inward-turning intake with tri-ducts for combined cycles engines for the operation of three different modes controlled by a single rotational flap on the compression side, which efficiently simplifies the inlet structure and the flap control mechanism. At high flight speed between Mach 4 and 6, the pure scramjet mode is switched on, whereas both the ejector and the scramjet paths are open for a moderate Mach number between 2 and 4 with a larger throat area guaranteeing the inlet startability. In the low flight speed range with Mach number below 2, the additional turbojet path will be turned on to provide air for the turbine engine, whereas the other two paths remain open for spillage. Results show that numerical simulations under different operation modes have proven the utility and good performance of the designed inlet. It could be stated because of a nearly full mass flow ratio and a total pressure recovery of around 0.5 that could be achieved at the cruise speed. Meanwhile, the intake works correctly at low flight speeds which overcomes the typical starting problem seen in intake designs.

In this scenario, the present work contributes to the state-of-art development of a scramjet intake by analyzing, through 3D CFD analysis, the effects of the change in different parameters of flight conditions. This work focus on the change in Mach number has on performance, total and static and static pressures. Contour images and values of properties along the walls were considered in the analyses. Three boundary conditions were examined considering Mach numbers of 6.8, 7.2, and 7.6. These Mach numbers were chosen because they represent quite well a common Mach number range of vehicles powered by scramjet engines. Results show that the most prominent consequence of an increase in Mach number is the increase in total pressure. This can be considered a relevant result once scramjet performance is directly related to the total pressure. Results have also shown that the Mach number change has an insignificant influence in the scramjet intake performance, measured through adiabatic kinetic efficiency. This is in accordance with Smart (Smart, 2012).

In this way, it is possible to state that this work gives its contribution to advance in this challenging field of designing an airbreathing engine to power hypersonic speed vehicles. All the numerical calculations in this work used the fluid dynamics ANSYS Fluent code. Therefore, the numerical methods and transitional viscous models used in this work were the ones available in Ansys Fluent (ANSYS, 2018).

2 – PROBLEM FORMULATION

The classical Navier Stokes equations for compressible flow has been considered. For a time-dependent fluid flow, Eq.(2.1) represents the mass balance, Eq.(2.2) to Eq. (2.4) the momentum balances in the x, y

and z directions, and Eq. (2.5) is the energy balance. In these equations, *u, v, w* refer to flow velocities in the x, y and z directions respectively. And *u* represents the total vectorial flow velocity that is obtained from the sum of the contributions of x, y, and z. The term Φ refers to the dissipation function, represented by Eq. (2.6) and μ is a viscosity term that relates the stresses to the volumetric deformation.

$$\nabla.(\rho u) = 0 \tag{2.1}$$

$$\nabla.(\rho uu) = -\frac{\partial p}{\partial x} + \nabla.(u\nabla u) + S_{Mx} \tag{2.2}$$

$$\nabla.(\rho vu) = -\frac{\partial p}{\partial y} + \nabla.(u\nabla y) + S_{My} \tag{2.3}$$

$$\nabla.(\rho wu) = -\frac{\partial p}{\partial z} + \nabla.(u\nabla w) + S_{Mz} \tag{2.4}$$

$$\nabla.(\rho c_p Tu) = -p\nabla.u + \nabla.(k\nabla \mathrm{T}) + \Phi + S_i \tag{2.5}$$

$$\Phi = \mu\left\{2\left[\left(\frac{\partial u}{\partial x}\right)^2 + \left(\frac{\partial v}{\partial y}\right)^2 + \left(\frac{\partial w}{\partial z}\right)^2\right] + \left(\frac{\partial u}{\partial y} + \frac{\partial v}{\partial x}\right)^2 + \left(\frac{\partial u}{\partial z} + \frac{\partial w}{\partial x}\right)^2 \left(\frac{\partial v}{\partial z} + \frac{\partial w}{\partial y}\right)^2\right\} + \lambda(\nabla.u)^2 \tag{2.6}$$

Because of the turbulent nature of the flow, the solver used in this work considers and adapted version of these equations. The turbulence model used in the calculations presented in this work is the Reynolds-averaged Navier Stokes (RANS) equations.

In the analyses presented in this work, the transition SST model was chosen as the turbulence model. This model is based on the combination of the SST k-ω transport equations with two other transport equations: intermittency and one for the transition onset criteria, in terms of momentum-thickness Reynolds number.

This work used the software Ansys Fluent for the calculations and more details of the equations can be found in the Ansys Fluent User's Guide (ANSYS, 2018). This software is reliable in many different areas including for the calculation of flows in hypersonic velocities, as it can be seen in the work of Sarout (Sarout et al, 2020). There are three models for transition prediction available in Ansys Fluent: transition SST model, intermittency transition model and transition k-kl model. In the work of Siqueira (Siqueira, 2016) a transition model validation was performed and the SST model presented to be more suitable for the calculations of compressible flows in a scramjet intake.

Yet this work analyzes the performance of the scramjet intake based on the flow conditions at the intake throat, or isolator. A typical parameter applied to quantify the intake compression performance is the kinetic energy efficiency, η_{KE}. The definition of η_{KE} is the ratio of the kinetic energy the compressed flow would achieve if it were expanded isentropically to freestream pressure, relative to the kinetic energy of the freestream. Figure 2.1 shows the Mollier diagram for a better visualization of the compression process in a scramjet intake (Waltrup et al., 1982).

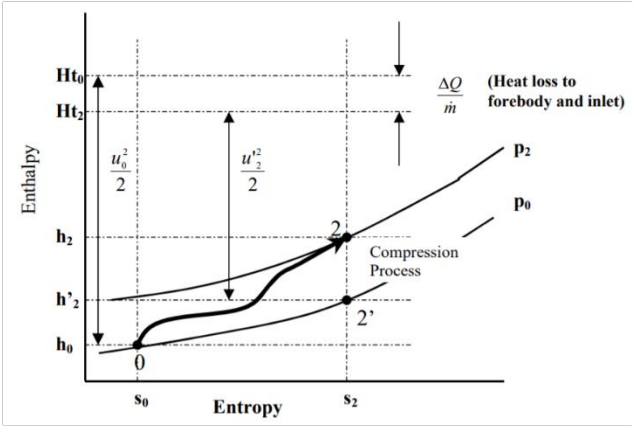

Figure 2.1 - Mollier diagram of intake compression process (Waltrup et al, 1982).

This work uses the adiabatic kinetic efficiency, η_{KE_ad}. In this case, it is not considered heat loss to the structure and is represented in Eq. (2.7).

$$\eta_{KE,ad} = \frac{H_{to} - h_2'}{H_{to} - h_0} \qquad 2.7$$

where H and h are total enthalpy and enthalpy related to the compression process presented by the Mollier diagram in Figure 1.

Waltrup has developed an empirical correlation in terms of the ratio of Mach number to freestream Mach number, M_2/M_0 (Waltrup et al., 1982). This expression associates intake efficiency to an intake capability parameter, M_2/M_0, so it meets the requirement for being a useful relation (Waltrup et al., 1982). Equation (2.8) represents this correlation:

$$\eta_{KE,ad} = 1 - 0.4\left\{1 - \frac{M_2}{M_0}\right\}^4 \qquad 2.8$$

Cases with three different Mach numbers have been considered in this analysis: 6.8, 7.2 and 7.6. All cases considered flight altitude of 30 km and angle of attack of +4°. Two wall temperatures are considered in this calculations: 800 K and 300 K for the triple wedge and isolator walls respectively. It is important to highlight that the sidewall at the coordinate z= 0 (left side of contour images) corresponds to the symmetry condition while the other sidewall features the actual wall condition. Figure 2.2 shows the computational domain considered for all calculations performed in this work.

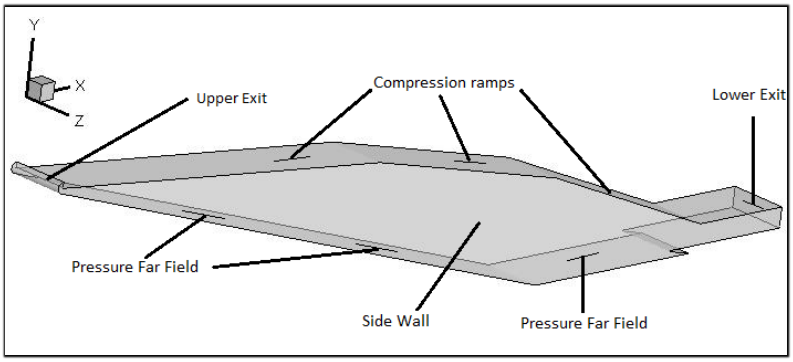

Figure 2.2 – Computational domain of a scramjet intake.

To guarantee mesh independence for the flow solution, a common mesh independence check has been done. Three mesh sizes have been created. It was considered a regular pressure distribution throughout the compression ramps. The region near the walls features more refined mesh for properly capturing the physical phenomena inside the boundary layer. Three different mesh sizes were simulated. The less refined mesh employed for this validation presented approximately 7 million elements (50% the size of the chosen mesh for this work) and the more refined mesh around 17.5 million elements (25% more elements than the used mesh in this work, which features around 14 million elements). Figure 2.3 displays the pressure along the whole compression ramps. Results show that the mesh refinement effects are more prominent on the end of the third ramp. Therefore, as a manner to align good accuracy with a reasonable computational time, the mesh with 14 million volumes has been chosen for all results shown in this study.

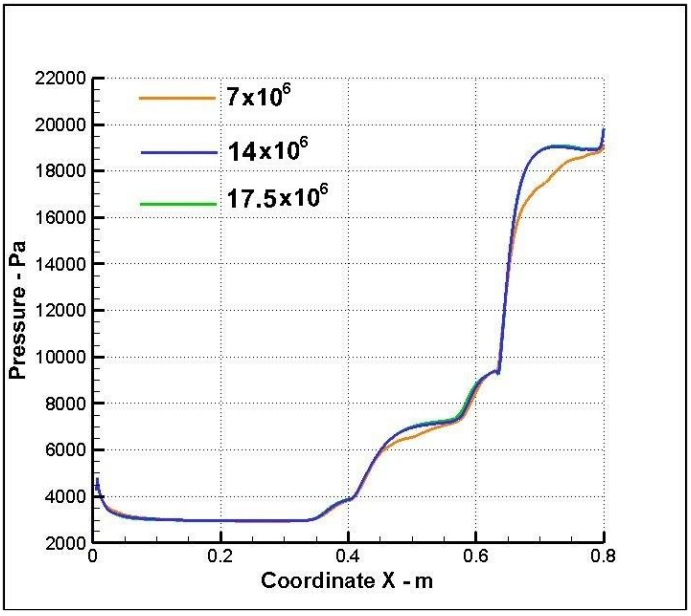

Figure 2.3 - Pressure along the compression ramps for cases with different number of elements.

3 - MACH NUMBER VARIATION ANALYSES

Results show that the Mach number does not influence much the airflow static pressure contour nor in the triple wedge neither in the isolator regions and therefore contour results are dismissed. Actually, results show that there is a minimal increase in static pressure as the Mach number gets higher. Figure 3.1 shows the values of static pressure along the compression ramps in the middle of the intake (60 mm far from the sidewall). Figure 3.1 presents results from the cases of Mach 6.8, 7.2, and 7.6. The pressure due to the shock wave on the vehicle leading edge, at the very beginning of the graph, is about 15000 Pa for the Mach 7.6 case. The pressure naturally decreases and because of the first compression, it goes around 5000 Pa. The following increases refer to the second and third compressions. The most significant pressure difference is about 8000 Pa at the end of the third ramp. This is a piece of relevant information once a scramjet intake is supposed to face high loads of pressure and certainly it will occur in this region. The pressure oscillation before every pressure increase is due to boundary layer separation in the corner between the ramps. Results also indicated that the static pressure distribution along the upper wall of the isolator is not so significant and is not presented in this work.

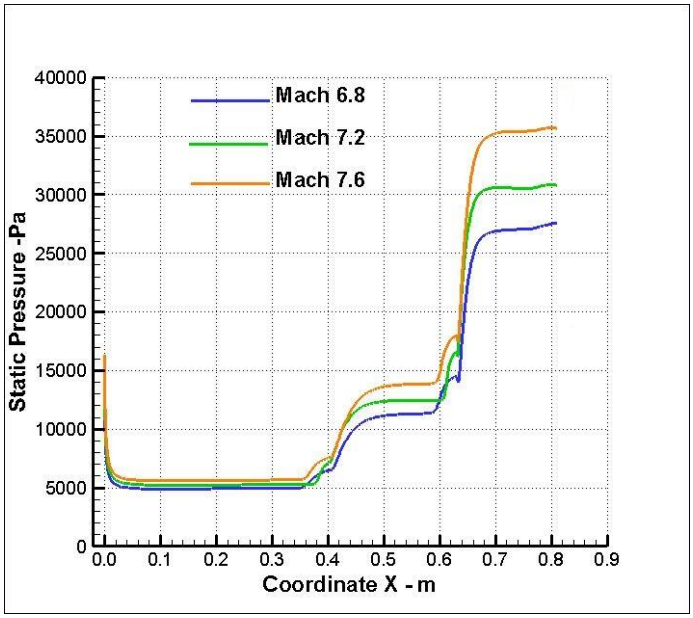

Figure 3.1 - Static pressure along the compression ramps for cases with different Mach numbers.

The following results show that the Mach number variation greatly changes the airflow total pressure in the scramjet intake. On the other hand, the total pressure distribution throughout the compression ramps and upper wall of the isolator is pretty much the same once the flow velocity is considered zero on the wall and therefore there is no dynamic pressure. In this way, the total pressure distribution on the walls isn't presented in this subsection. The cases analyzed in this subsection are the same analyzed in the last one: Mach numbers of 6.8, 7.2, and 7.6. There is a considerable total pressure variation in these cases and as a consequence the contour results considered different total pressure ranges, otherwise, it would be impossible to visualize any contour results. In this way, Fig. 3.2, 3.3 and 3.4 represent the total pressure contour of a case with Mach number 6.8, 7.2 and 7.6 which features a maximum total pressure of 4.0 $x10^6$ Pa, 5.5 $x10^6$ and 7.5$x10^6$ Pa respectively. The huge total pressure difference among the cases with different Mach numbers is not seen inside the isolator and therefore the maximum total pressure considered in all cases is also 7.5$x10^6$ Pa. Figures 3.5, 3.6 and 3.7 show the total pressure contour for the case with Mach number 6.8, 7.2 and 7.6 respectively. Results suggest that greater Mach numbers make the total pressure also increase inside the isolator. The big boundary layer separation located at the beginning of the upper wall produces a region of lower total pressure. As the airflow goes through the isolator its total pressure goes down (it can be seen on the second isolator slice). Sidewall viscous effects also decrease the total pressure and affect the airflow structure. This analysis of the total pressure is relevant information once higher airflow total pressure contributes to a better performing intake. For all cases, some flow characteristics are the same such as viscous effects near the walls (both ramps and sidewall) and lower total pressure as the airflow is affected by the shock waves. In summary, these results are in accordance with what was expected: the higher Mach number the higher the total pressure once the Mach number increase results in greater dynamic pressure that consequently would increment the overall total pressure.

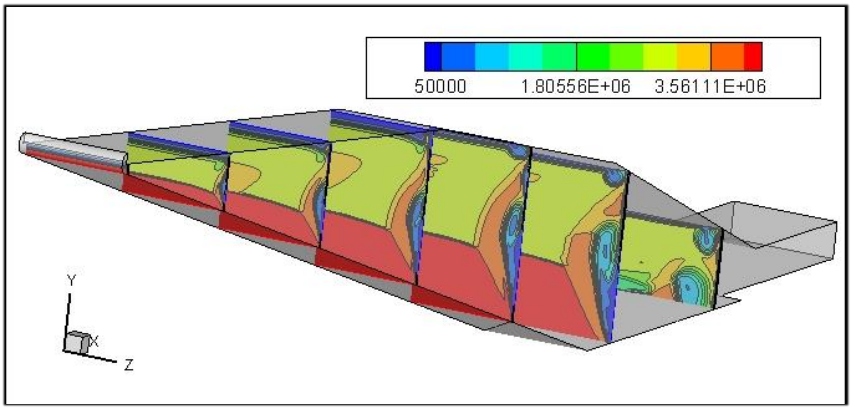

Figure 3.2 - Total pressure contour of the compression ramps region of a Mach 7.6 case considering maximum total pressure of 7.5 $x10^6$ Pa.

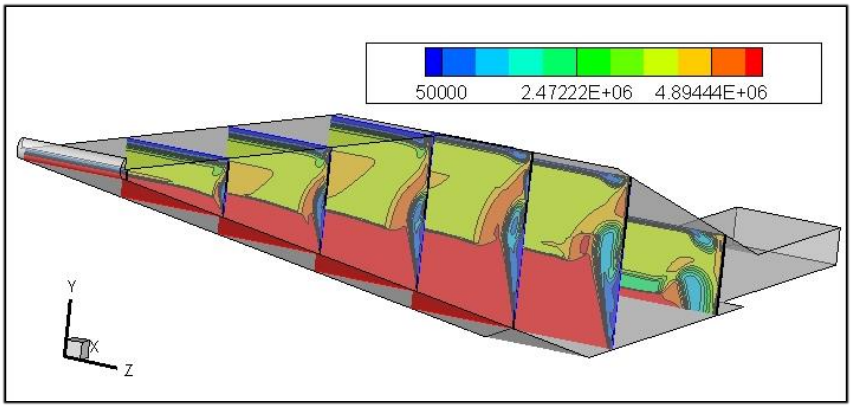

Figure 3.3 - Total pressure contour of the compression ramps region of a Mach 7.2 case considering maximum total pressure of 5.5 $x10^6$ Pa.

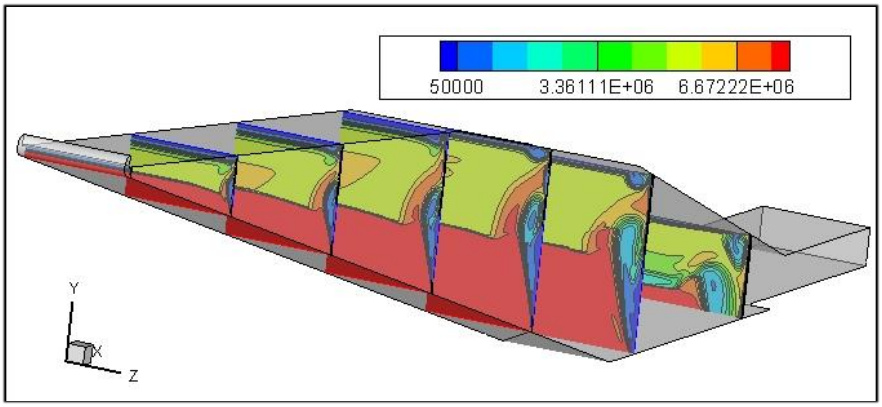

Figure 3.4 - Total pressure contour of the compression ramps region of a Mach 7.6 case considering maximum total pressure of 7.5 x10^6 Pa.

The following figures show contour results of the total pressure inside the isolator. Results show that greater Mach numbers make the total pressure also increase inside the isolator. The big boundary layer separation located at the beginning of the upper wall produce a region of lower total pressure. As the airflow goes through the isolator its total pressure goes down. Sidewall viscous effects also decreases the total pressure. These results are very important because the airflow is directed to the combustion chamber as soon as it leaves the isolator.

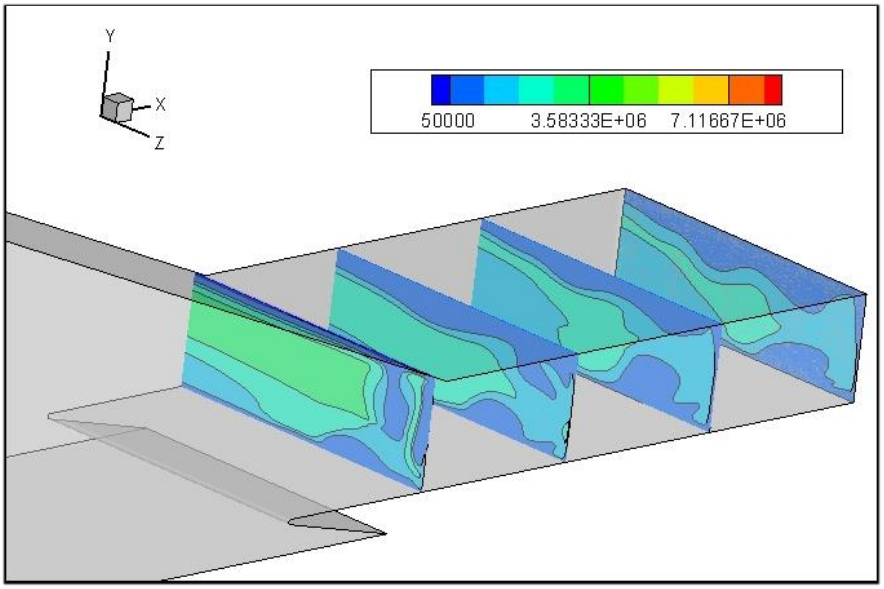

Figure 3.5 - Total pressure contour of the isolator region of a Mach 6.8 case.

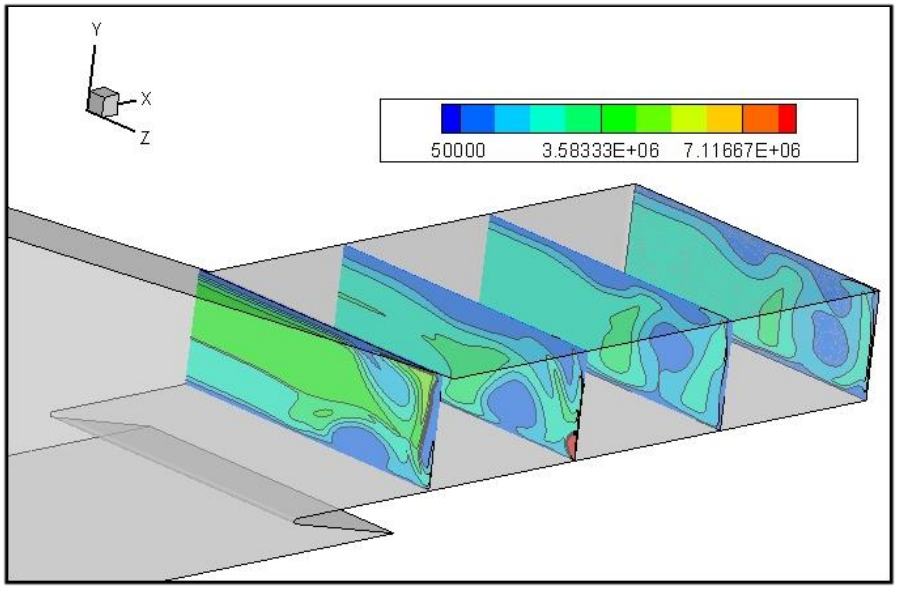

Figure 3.6 - Total pressure contour of the isolator region of a Mach 7.2 case.

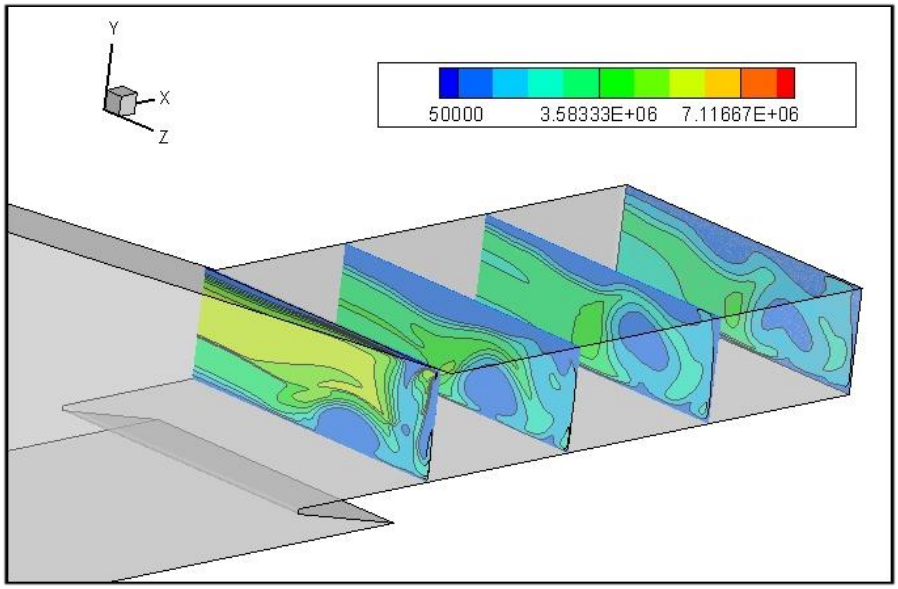

Figure 3.7 - Total pressure contour of the isolator region of a Mach 7.6 case.

The overall scramjet inlet performance in terms of adiabatic kinetic efficiency, which is represented by Eq. (3.8), for different Mach numbers shown in these analyses is displayed in Fig. 3.8. It is important to remember that this parameter does not account for heat loss to the structure. The empirical correlation proposed by Waltrup, and represented by Eq. (3.8) is shown in the results for the sake of comparison (Waltrup et al, 1982). Results indicate, at first, the Mach number variation presented in this analysis does not affect much the scramjet efficiency, which very slightly increases as the Mach number goes up. In fact, according to Smart (Smart, 2012) this parameter value is relatively independent of flight Mach number for this kind of scramjet intake and it explains such small and imprecise variation in this result.

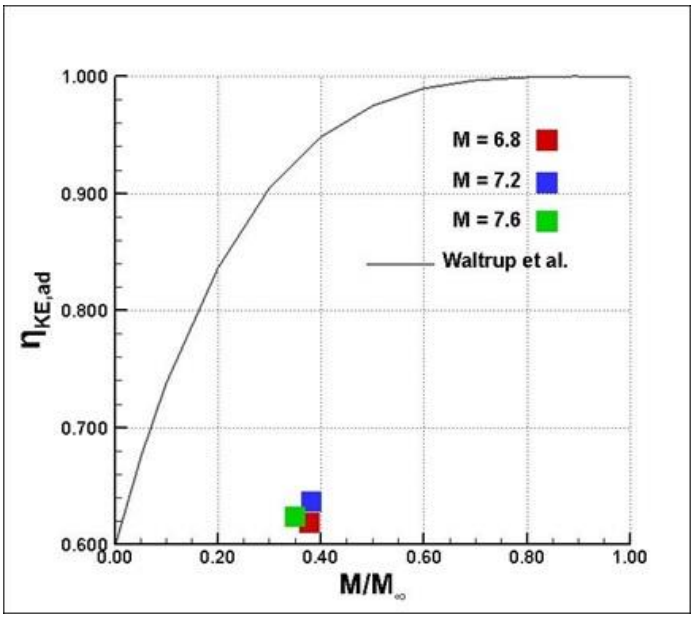

Figure 3.8 – Adiabatic kinetic efficiency of scramjet intakes considering different Mach numbers.

4. CONCLUSION

In this work, the variation of the Mach number has been investigated on how they affect the airflow in a scramjet intake (compression ramps and isolator). Each parameter influences the airflow differently. Contour images and values of the properties on the walls have been considered in these investigations. The properties considered to analyze the airflow behavior are Mach number, static pressure and total pressure. Yet, it was analyzed the influence of these parameters on the intake performance through the measure of adiabatic kinetic efficiency. Some characteristics of the intake are the same for all cases: blunt-leading-edge radii of 0.5 mm and isolator height of 20 mm. Yet transition SST model has been considered in all cases and wall temperatures of 800 K and 300 K on the triple wedge and isolator regions respectively.

Three Mach numbers have been considered in the first analyses of this work: 6.8, 7.2, and 7.6. In each of the three cases is possible to visualize the great influence of the sidewall on the airflow. In these first results, it is possible to notice that viscous effects along the sidewall considerably affect the airflow in the intake. Complex shock-wave boundary-layer interactions, which happen in the region near the sidewall, make the Mach number to decrease. Considering the pressure values along the compression ramps, it is possible to state that greater Mach numbers generate higher pressure on the walls. The pressure on the wall increase after every compression ramp and, at the third ramp the pressure difference is more prominent between Mach 6.8 and 7.6 cases: around 8000 Pa. The analysis in the isolator suggests that the pressure inside of it also increases as the Mach number goes up. Considering the pressure values on the upper wall of the isolator, results also indicate that the higher the Mach number the higher the pressure on the wall. The intake of an air-breathing hypersonic vehicle is supposed to deal with very high loads of pressure and therefore this analysis is worth doing once it can map the location of higher pressures. That certainly will help in the design of such type of engine. Considering the effects of Mach number on total pressure in different parts of the scramjet intake through contour images, it is possible to state that the Mach number affects quite a lot the total pressure in the intake. There is a noteworthy total pressure variation in these cases. The total pressure of the Mach 6.8 case is 4.0 $x10^6$ and increases up to 5.5 $x10^6$ Pa for the Mach 7.2 case and up to 7.5 $x10^6$ Pa for the Mach 7.6 case. For the isolator region, the overall total pressure also increases as the Mach number goes up. The airflow, after being compressed in the isolator, goes to the combustion chamber and need to be at ideal conditions so that the combustion process can start. Therefore, the analysis of this condition inside the isolator is quite relevant. At last, this work analyzed the effects that the Mach number variation has on the intake performance. It was measured by through the adiabatic kinetic efficiency. Results showed that the influence of the Mach number variation on it is insignificant.

4 ACKNOWLEDGEMENTS

This work is part of a longstanding research program supported by the Brazilian Air Force. The technical support of the Institute of Advanced Studies (IEAv) is highly acknowledged. The financial support provided by the CAPES-PROAP program is also appreciated.

5. REFERENCES

ALCAIDE, R. L. M. **Investigação da Combustão Supersônica em Túnel de Choque Hipersônico**. 2007. 97f. Thesis (Master in Science) – Instituto Tecnológico de Aeronáutica, São José dos Campos.

ANSYS, ANSYS Fluent 19.0 user's guide, Canonsburg, 2018.

BERTIN, J.J. **Hypersonic aerothermodynamics.** Washington, DC: AIAA, 1994. 608 p. (AIAA education series).

GRIFFITHS, A. D. **Development and Demonstration of a Diode Laser Sensor for a Scramjet Combustor**. 2005. Thesis (Doctor of Philosophy) – The Australian Natonal University, Australia.

HEISER, W. H.; PRATT, D. T. **Hypersonic Airbreathing Propulsion**. Reston, VA: AIAA, 1994.

IM S.; Do H. **Unstart phenomena induced by flow choking in scramjet inlet-isolators.** In: Progress in Aerospace Sciences 97.2 (2018), pp. 1 – 21. ISSN: 0376-0421.

JAVED, A.; CHAKRABORTY, D. **Evaluation of side spillage for a hypersonic air intake using computational fluid dynamic techniques.** *Proceedings of the Institution of Mechanical Engineers, Part G: Journal of Aerospace Engineering* (2017), 231(11), 2111–2119.

SAROUT, Y., R, T. K. R., Paramasivam, S. (2020). **Numerical Simulation of Flow through Scramjet Inlet - Isolator Model with Pressure Feedback.** AIAA Scitech 2020 Forum.

SEGAL, C. **The Scramjet Engine: Process and Characteristics**. 1st ed. Cambridge: Cambridge University Press, 2009. 270 p.

SENTHILKUMAR, P.; Chandram, S.; Sadasivan, S.; Govindha, N.; Kumar, S. **Effect of Cowl Angle in the Performance of Scramjet Air Intakes.** In: *International Journal of Mechanical Engineering and Technology (IJMET).* Volume 8, Issue 11, November 2017, pp. 899–909, Article ID: IJMET_08_11_09.

SIQUEIRA, J. V. M. B. **A computational study of the leading-edge bluntness and isolator on the 14-X scramjet intake.** 2016. 138f. Thesis (Master in Science) – Instituto Tecnológico de Aeronáutica, São José dos Campos.

SIQUEIRA, J. V. M. B., Rosa, M. A. P., & Ribeiro, G. B. (2020). **Numerical evaluation of effects of the isolator height and the leading-edge bluntness on a scramjet inlet.** In: *Journal of the Brazilian Society of Mechanical Sciences and Engineering (2020), 42(6).*

SMART, M. K. **How Much Compression Should a Scramjet Inlet Do?** In: AIAA J. 50.3 (2012), pp . 610–619. ISSN: 1533-385X.

WALTRUP P. J., BILLG F.S., STOCKBRIDGE R.D., 1982, **Engine sizing and integration requirements for hypersonic airbreathing missile applications**, AGARD-CP-207, No. 8.

ZHU, C., Zhang, X., Kong, F., & You, Y. (2018). **Design of a Three-Dimensional Hypersonic Inward-Turning Inlet with Tri-Ducts for Combined Cycle Engines**. In: *International Journal of Aerospace Engineering, 2018, 1–10.*

6. RESPONSIBILITY NOTICE

The authors are the only responsible for the printed material included in this paper.